



## Research article

# Impact of an effective Prandtl number model on the flow of nanofluids past an oblique stagnation point on a convective surface

Zafar Mahmood<sup>a</sup>, Sayed M. Eldin<sup>b</sup>, Amal F. Soliman<sup>c,d</sup>, Taghreed A. Assiri<sup>e</sup>, Umar Khan<sup>a,\*</sup>, S.R. Mahmoud<sup>f</sup>

<sup>a</sup> Department of Mathematics and Statistics, Hazara University, Mansehra, Pakistan

<sup>b</sup> Center of Research, Faculty of Engineering, Future University in Egypt New Cairo 11835, Egypt

<sup>c</sup> Department of Mathematics, College of Arts and Sciences, Prince Sattam bin Abdulaziz University, Wadi Addawasir, Saudi Arabia

<sup>d</sup> Department of Basic Science, Benha Faculty of Engineering, Benha University, Benha, Egypt

<sup>e</sup> Department of Mathematics, Faculty of Science, Umm Al-Qura University, Makkah, Saudi Arabia

<sup>f</sup> GRC Department, Applied College, King Abdulaziz University, Jeddah 21589, Saudi Arabia



## ARTICLE INFO

## Keywords:

Effective Prandtl number  
Gamma alumina nanofluid  
Convective surface  
Oblique stagnation point  
Numerical simulation

## ABSTRACT

The stretched surface's convective heat transfer capability can be improved by using nanoparticles. There is a significant role of the Prandtl number in determining the thermal and momentum stretching layer surfaces. It is proposed in this study that an effective Prandtl number model be used to explore the two-dimensional oblique stagnation point flow of  $\gamma Al_2O_3 - H_2O$  and  $\gamma Al_2O_3 - C_2H_6O_2$  nanofluids moving over a convective stretching surface. The fluid in question is subjected to a thorough investigation. It is necessary to apply non-linear ordinary differential equations in order to connect the controlling partial differential equations with the boundary conditions. To solve these equations, an efficient and reliable numerical technique is used. Shooting Method with Runge Kutta-IV in Mathematica software. Visual representations of normal and tangential velocity and temperature as well as streamlines as a function of many physical parameters are shown. The results show that as the volume fraction of nanoparticles increases, the fluid flow  $f(y)$ ,  $h(y)$  and velocity  $f'(y)$ ,  $h'(y)$  all increase, whereas the flow  $f(y)$  and velocity  $f'(y)$  both increase against the stretching ratio parameter, while the flow  $h(y)$  and velocity  $h'(y)$  both decrease. When the volume percentage of nanoparticles and the Biot number are both increased, the temperature rises. However, when the stretching ratio parameter is increased, the temperature falls. Physical attributes like the local skin friction coefficient and the heat flow may be characterized in many ways. A nanofluid comprised of  $\gamma Al_2O_3 - C_2H_6O_2$  outperformed a  $\gamma Al_2O_3 - H_2O$  nanofluid in terms of heat transfer rate. The source of zero skin friction may be observed to move to the left or right depending on the balance of obliqueness and straining motion at point  $x_s$ . The computed numerical results of the current research correspond well with those accessible in the literature for the limiting scenario.

\* Corresponding author.

E-mail address: [umar\\_jadoon4@yahoo.com](mailto:umar_jadoon4@yahoo.com) (U. Khan).

<https://doi.org/10.1016/j.heliyon.2023.e13224>

Received 12 July 2022; Received in revised form 20 January 2023; Accepted 20 January 2023

Available online 25 January 2023

2405-8440/© 2023 The Authors. Published by Elsevier Ltd. This is an open access article under the CC BY-NC-ND license (<http://creativecommons.org/licenses/by-nc-nd/4.0/>).

## 1. Introduction

In many industrial operations, such as the lamination of epoxy resins, the manufacturing of insulating materials, and the application of coating layers to stiff structures, stagnation point flows on stretched surfaces are used [1]. In the last several decades, these flows have been the subject of much attention, and their applications are many [2,3]. There is a substantial link between the thermal performance at a stretched surface as well as the final look of some technological operations, including pulp manufacturing, crystal manufacturing, and milling machines, among other things. The problem of momentum and heat transmission near the stagnation point is both theoretical and practical. So, being able to control the rate at which heat is transmitted at the interface is quite useful [4–7].

It has been shown again and again that the collision of the fluid with the wall, either orthogonally or at some other angle of occurrence, gives rise to the stagnation point flow that characterizes the point of stagnation. The production of papyrus, gemstone inflating, revolving threads, and molten whirling all include certain sorts of flows that pass over a stretched surface. These flows, which take heat transmission into consideration, are obvious. There are various industrial processes and applications that rely on stagnation point flow, like dip coating and metallic molding. In the area of the stagnation point flow, the pressure gradient and heat transfer are both seen to be at their highest levels [8]. Fig. 1 illustrates that the fluid hits a stretching surface at an arbitrary angle of incidence and that the fluid away from the surface travels with the free stream velocity  $u = ax + by$  (where  $x$  and  $y$  are coordinates along the  $x$ -axis and the  $y$ -axis, respectively, and  $a$  and  $b$  are dimensional constants with dimension  $[1/T]$ ). This information may be found by referring to the figure.

The sustained 2-D oblique flow of a viscous liquid at its stagnation point has been researched by a number of researchers. Stuart [9] originated this field, which was further investigated by Tamada [10] and Dorrepaal [11]. By incorporating a stretched surface, Reza and Gupta [12] generalized Chiam's issue [13]. During their research, they didn't take into account factors like dispersion depth and strain gradients. Lok et al. [14], study resulted in a partial solution to this challenge. Reza and Gupta [15] corrected the mistakes in Refs. [12,14] and came up with the proper answer. Tooke and Blyth [16,17] included an unconstrained measurement connected to an external component that was linked to the pressure distribution in their models. It was discovered by Putkaradze and Weidman [18,19] that a circular stagnation point flow intruding on a stable oblique stagnation point flow might occur.

In order to characterize the flow, a number of boundary value problems are combined and solved. "Orthogonal and oblique stagnation point flows have been extensively studied by Refs. [20–25]." According to a recent study by Ahmed et al. [26], viscoelastic nanomaterials approaching the stagnation point on a stretched disc exhibit time-dependent flow. Nadeem et al. [27] "investigated 2-D oblique stagnation point flow of a CNT-based fluid over a convective surface." From a great number of perspectives in the field of fluid dynamics, including those of scientists and researchers, the oblique stagnation point flow of a nanofluid towards a stretching or shrinking surface has been contemplated from a variety of perspectives [8,28,29].

Nanofluids have garnered a lot of attention over the last several decades. The relevance of this field throughout cosmetics and medical processing, metabolic stress, biofuel, nanotechnology, cross-breed fuel-powered motors, antifreeze for sophisticated reactors, and several other fields of study has resulted in numerous contributions [30–32]. By employing nanoparticles to increase heat conductivity, Maxwell [33] outlined a fundamental concept. The term "nanofluid" was coined in 1995 by Choi [34] as the first to characterize a fluid. His research focused on the characteristics of nanofluids, and he discovered that metallic particles may boost the heat conductivity of the underlying fluid. In the manufacture of nanoparticles, a broad range of materials are employed. All metals (such as aluminum), metal cladding (like silicon dioxide), and nonmetals (such as graphite carbon nanotubes) are included.

Because of their exceptional thermal and mechanical characteristics, nanomaterials are becoming more significant [35]. These materials have a significant impact on the characteristics of the nanofluids that are produced by each individual nanomaterial. There is a class of substances called aluminum  $Al_2O_3$  alloys that fall within the category of nanomaterials. A major contribution from aluminum may be found in these alloys. Heat-treatable aluminum ( $Al_2O_3$ ) alloys are distinguished from non-heat-treatable aluminum alloys by their ability to undergo heat treatment [36].

When trying to increase the thermal conductivity of nanoliquids, alumina, also known as aluminum oxide ( $Al_2O_3$ ), is the nanosized particle that is used most often. Researchers have been interested in the use of  $Al_2O_3$  nanoliquid as a result of its potential use in a

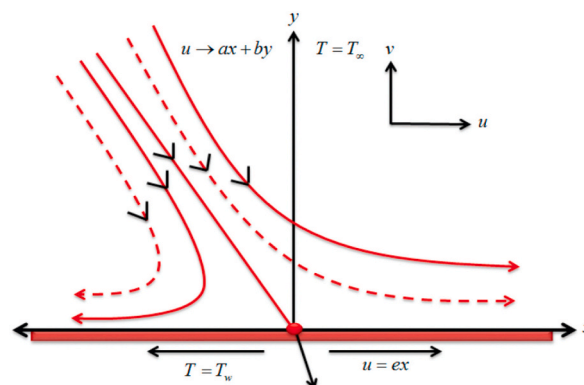


Fig. 1. Description of the dilemma in relations of its physical characteristics.

variety of freezing procedures. According to the magnitudes of their sizes, nanoscale  $Al_2O_3$  particles may be allocated into two distinct types:  $\alpha Al_2O_3$  and  $\gamma Al_2O_3$ . Maciver et al. [37] looked at the attributes of two different types of alumina models: eta and gamma.

The significance of  $Al_2O_3$  nanofluids in cooling operations was uncovered by Sow [38] via preliminary research into the flow dynamics of these fluids. According to the research carried out by Vishnu Ganesh et al. [39] and Rashidi et al. [40], the flow properties of  $\gamma Al_2O_3$  nanofluids may be analyzed using similarity solutions. In their investigations, they made use of experimentally derived thermophysical parameters. Rashidi et al. [40] investigated the effects of an efficient  $Pr$  on the flow of an  $\gamma Al_2O_3$  nanofluid and found that the temperature of the  $\gamma Al_2O_3$  nanofluids was significantly affected.

A comprehensive review of the literature has shown that nobody has looked at how an experimentally derived Prandtl number model effects  $\gamma Al_2O_3 - H_2O$  and  $\gamma Al_2O_3 - C_2H_6O_2$  nanofluid’s thermal performance while it’s being flown obliquely across the convective layer of a stretched convection surface of stagnation point flow so far. So, we tried to fill this gap by considering this research. The current study investigated the flow and heat transfer properties of an incompressible  $\gamma Al_2O_3 - H_2O$  and  $\gamma Al_2O_3 - C_2H_6O_2$  nanofluid across a stretched convective surface using an oblique stagnation point flow of steady two-dimensional laminar flow with an efficient Prandtl number model. An effective Prandtl number model [40] was used in the present investigation to determine ultimate outcomes. Both with and without an effective Prandtl number flow, these non-linear ordinary differential equations are quantitatively determined. Shooting with RK-IV techniques in the computation software MATHEMATICA is used for computational work. In contrast to the research that was accessible in the past, the offered model is shown in Table 1 with its exact degree of originality highlighted. Despite the wide range of relevant parameter values, the tables and figures show typical flow, streamlines pattern, temperature, and velocity profiles, as well as the placement of zero-skin friction in the vicinity. The purpose of this evaluation is to ensure the responses to the following questions, which are as follows:

- What is the stimulus of nanoparticles volume fraction over with and without effective Prandtl number model for velocity profile of convective surface?
- What effect do nanoparticles have on the thermal distribution of a convective surface when an effective Prandtl number or without effective Prandtl number model is used?
- What is the effect of Biot number parameter, velocity ratio parameter and other physical parameters on respective profiles?

It is feasible that this will be useful in research carried out in the potential to increase the effectiveness of heat transfer in modern manufacturing environments.

The issue is mathematically stated in the next section.

## 2. Model formulation

An oblique stagnation point flow of  $\gamma Al_2O_3 - H_2O$  and  $\gamma Al_2O_3 - C_2H_6O_2$  nanofluid is considered to occur over a convective stretching surface in this work. Let’s pretend that flow is steady, laminar, and two-dimensional in nature. The  $y$ -axis is perpendicular to the wall, whereas the surface is extended along the  $x$ -axis (see Fig. 1). Updraft equilibrium is predicted for the base fluids and alumina. Furthermore, the surface temperature  $T_f$  and the ambient temperature  $T_\infty$  have been taken into account. Thermophysical characteristics are given in Table 2. Model simulation is Presented in Fig. 2.

The following are the flow equations, based on the previously stated assumptions [8,27]:

$$\frac{\partial u^*}{\partial x^*} + \frac{\partial u^*}{\partial y^*} = 0, \tag{1}$$

$$u^* \frac{\partial u^*}{\partial x^*} + v^* \frac{\partial u^*}{\partial y^*} + \frac{1}{\rho_{nf}} \frac{\partial p^*}{\partial x^*} = \nu_{nf} \nabla^{*2} u^*, \tag{2}$$

$$u^* \frac{\partial v^*}{\partial x^*} + v^* \frac{\partial v^*}{\partial y^*} + \frac{1}{\rho_{nf}} \frac{\partial p^*}{\partial y^*} = \nu_{nf} \nabla^{*2} v^*, \tag{3}$$

$$u^* \frac{\partial T^*}{\partial x^*} + v^* \frac{\partial T^*}{\partial y^*} = \alpha_{nf}^* \frac{\partial^2 T^*}{\partial y^{*2}} \tag{4}$$

**Table 1**  
Analysis of the available literature to determine the novelty of the model.

Authors	Oblique Stagnation Point	Nanofluids		Without and With Effective Prandtl Model
		$\gamma Al_2O_3 - H_2O$	$\gamma Al_2O_3 - C_2H_6O_2$	
Ghaffari et al. [28]	✓	×		×
Mandal et al. [29]	✓	×		×
Nadeem et al. [27]	✓	×		×
Ramzan et al. [8]	✓	×		×
Present work	✓	✓		✓

**Table 2**  
Thermal and physical characteristics of the three hydrocarbons H<sub>2</sub>O, C<sub>2</sub>H<sub>6</sub>O<sub>2</sub> and Al<sub>2</sub>O<sub>3</sub>([40]).

	$\rho(\text{kg}/\text{m}^3)$	$C_p(\text{J}/\text{kgK})$	$k(\text{W}/\text{m K})$	$Pr$
Pure Water (H <sub>2</sub> O)	998.3	4182	0.60	6.96
Ethylene glycol (C <sub>2</sub> H <sub>6</sub> O <sub>2</sub> )	1116.6	2382	0.249	204
Alumina (Al <sub>2</sub> O <sub>3</sub> )	3970	765	40	

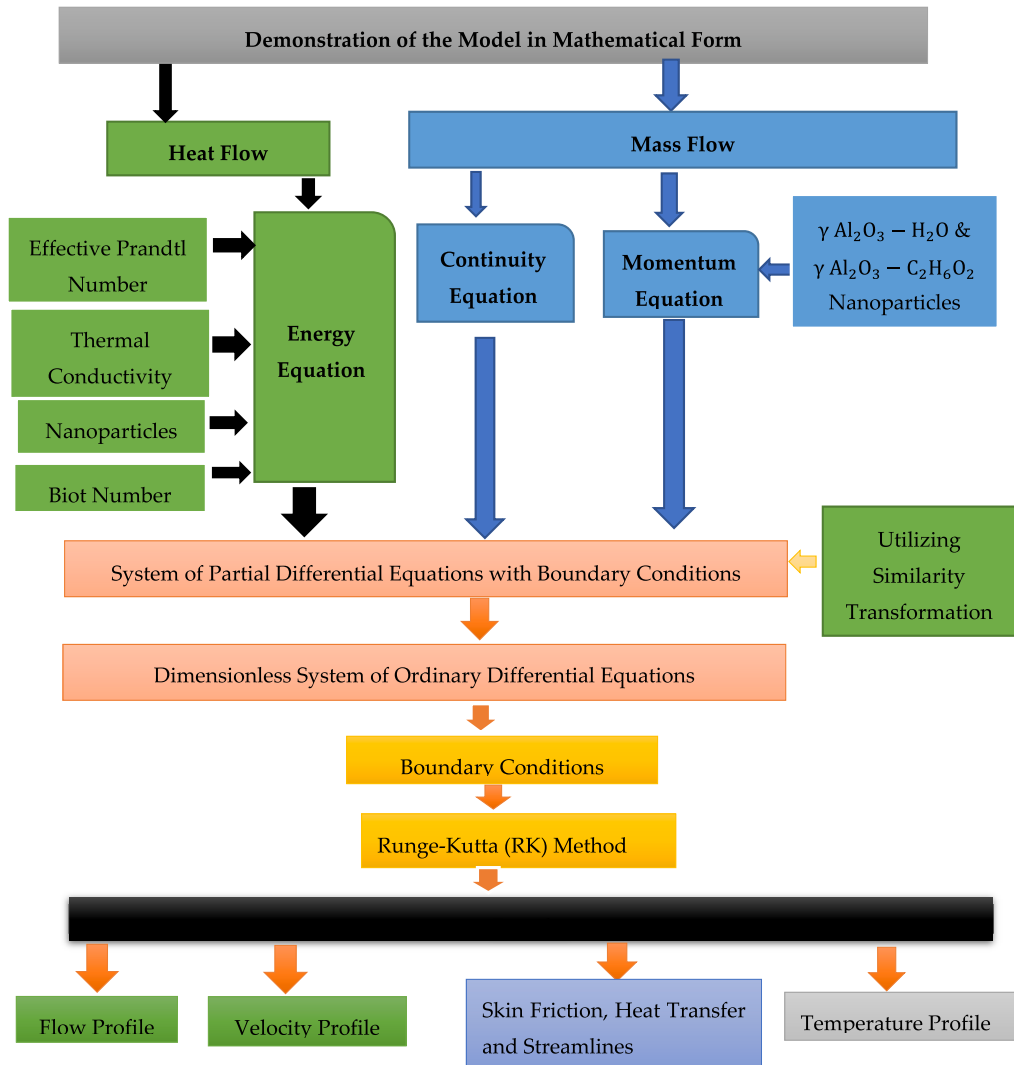


**Fig. 2.** Model simulation.

The  $x$ - and  $y$ -axis of velocity components are signified by  $u^*$  and  $v^*$ ,  $T^*$  is the temperature, the kinematic viscosity is represented by  $\nu_{nf}$ , and the effective thermal diffusivity of the nanofluid is represented by  $\alpha_{nf}^*$ . If one of the following criteria exists (see Ref. [27]):

$$\left. \begin{aligned} u^* &= cx^*, -k \frac{\partial T^*}{\partial y^*} = h_f(T_f - T^*) \text{ at } y^* = 0 \\ u^* &= ax^* + by^*, T \rightarrow T_\infty \text{ as } y^* \rightarrow \infty \end{aligned} \right\} \quad (5)$$

Here the variables  $a$ ,  $b$ , and  $c$  are all positive quantities with inverse time dimensions,  $h_f$  is the convective heat transfer coefficient, and the variable  $c > 0$  indicates stretching. By employing (see Ref. [27])



here

$$\dot{A} = 123\varphi^2 + 7.3\varphi + 1 \text{ (for } \gamma \text{ Al}_2\text{O}_3 - \text{H}_2\text{O)},$$

$$\dot{A} = 360\varphi^2 - 0.19\varphi + 1 \text{ (for } \text{Al}_2\text{O}_3 - \text{C}_2\text{H}_6\text{O}_2)$$

and.

$$\overline{\mathcal{H}} = \frac{\text{Pr}_f \left( (1-\varphi) + \varphi \frac{\rho_s}{\rho_f} (82.1\varphi^2 + 3.9\varphi + 1) \right)}{123\varphi^2 + 7.3\varphi + 1} \text{ (With effective Pr for } \gamma \text{ Al}_2\text{O}_3 - \text{H}_2\text{O)},$$

$$\overline{\mathcal{H}} = \frac{\text{Pr}_f \left( (1-\varphi) + \varphi \frac{\rho_s}{\rho_f} (254.3\varphi^2 - 3\varphi + 1) \right)}{306\varphi^2 - 0.19\varphi + 1} \text{ (With effective Pr for } \gamma \text{ Al}_2\text{O}_3 - \text{C}_2\text{H}_6\text{O}_2)$$

$$\overline{\mathcal{H}} = \frac{\text{Pr}_f \left( 1 - \varphi + \varphi \left( \frac{\rho_s c_{p,s}}{\rho_f c_{p,f}} \right) \right)}{4.97\varphi^2 + 2.72\varphi + 1} \text{ (Without effective Pr for } \gamma \text{ Al}_2\text{O}_3 - \text{H}_2\text{O)}$$

$$\overline{\mathcal{H}} = \frac{\text{Pr}_f \left( 1 - \varphi + \varphi \left( \frac{\rho_s c_{p,s}}{\rho_f c_{p,f}} \right) \right)}{28.905\varphi^2 + 2.8273\varphi + 1} \text{ (Without effective Pr for } \gamma \text{ Al}_2\text{O}_3 - \text{C}_2\text{H}_6\text{O}_2)$$

It's also worth noting that the boundary conditions

$$\left. \begin{aligned} f(0) = 0, f'(0) = 1, f'(\infty) = \frac{a}{c}, \\ g(0) = 0, g'(0) = 0, g''(\infty) = \gamma = \frac{b}{c}, \\ \theta'(0) = -Bi(1 - \theta(0)), \theta(\infty) = 0 \end{aligned} \right\} \tag{18}$$

Here  $Bi = \frac{h}{k} \sqrt{\frac{\mu}{\rho c}}$  is the Biot number,  $f(y)$  operates as  $(\frac{a}{c})y + A$  as  $y \rightarrow \infty$ , according to a study of the flow governing system. Where  $A$  denotes the boundary displacement constant, which fluctuates with changes in the flow's other relevant characteristics.

Substituting Eq. (18) in above, we get

$$C_1 = \left[ (1 - \varphi) + \varphi \frac{\rho_s}{\rho_f} \right] \left( \frac{a}{c} \right)^2 \text{ and } C_2 = -A\gamma \left[ (1 - \varphi) + \varphi \frac{\rho_s}{\rho_f} \right].$$

To begin with (see Refs. [8,27])

$$g'(y) = \gamma h(y) \tag{19}$$

Equations (15)–(18) have the subsequent form

$$\frac{1}{A} f''' + \left[ (1 - \varphi) + \varphi \frac{\rho_s}{\rho_f} \right] (ff'' - f'^2) + \left( \frac{a}{c} \right)^2 = 0, \tag{20}$$

$$\frac{1}{A} h'' + \left[ (1 - \varphi) + \varphi \frac{\rho_s}{\rho_f} \right] (fh' - f'h - A) = 0, \tag{21}$$

$$\theta'' + \overline{\mathcal{H}}(f\theta') = 0. \tag{22}$$

Where  $\dot{A}$  and  $\overline{\mathcal{H}}$  discussed above. And the boundary conditions (see Ref. [27])

$$\left. \begin{aligned} f(0) = 0, f'(0) = 1, h(0) = 0, \theta'(0) = -Bi(1 - \theta(0)), \\ f'(\infty) = \frac{a}{c}, h'(\infty) = 1, \theta(\infty) = 0. \end{aligned} \right\} \tag{23}$$

A number of important physical parameters, including shear stress and local thermal transfer at the extended convective surface, are described in non-dimensional form by the following equations (see Refs. [27,40]):

$$\tau_w = \frac{\mu_{nf}}{\mu_f} (x\Gamma''(0) + \gamma h'(0)) \text{ (for } \gamma \text{ Al}_2\text{O}_3 - \text{H}_2\text{O and } \gamma \text{ Al}_2\text{O}_3 - \text{C}_2\text{H}_6\text{O}_2) \tag{24}$$

$$q_w = -\frac{k_{nf}}{k_f} [\theta'(0)] \text{ (for } \gamma \text{ Al}_2\text{O}_3 - \text{H}_2\text{O and } \gamma \text{ Al}_2\text{O}_3 - \text{C}_2\text{H}_6\text{O}_2) \tag{25}$$

When the wall shear stress is zero, the stagnation point  $x_s$  may be reached, i.e.

$$x_s = -\gamma \frac{h'(0)}{f''(0)}, \tag{26}$$

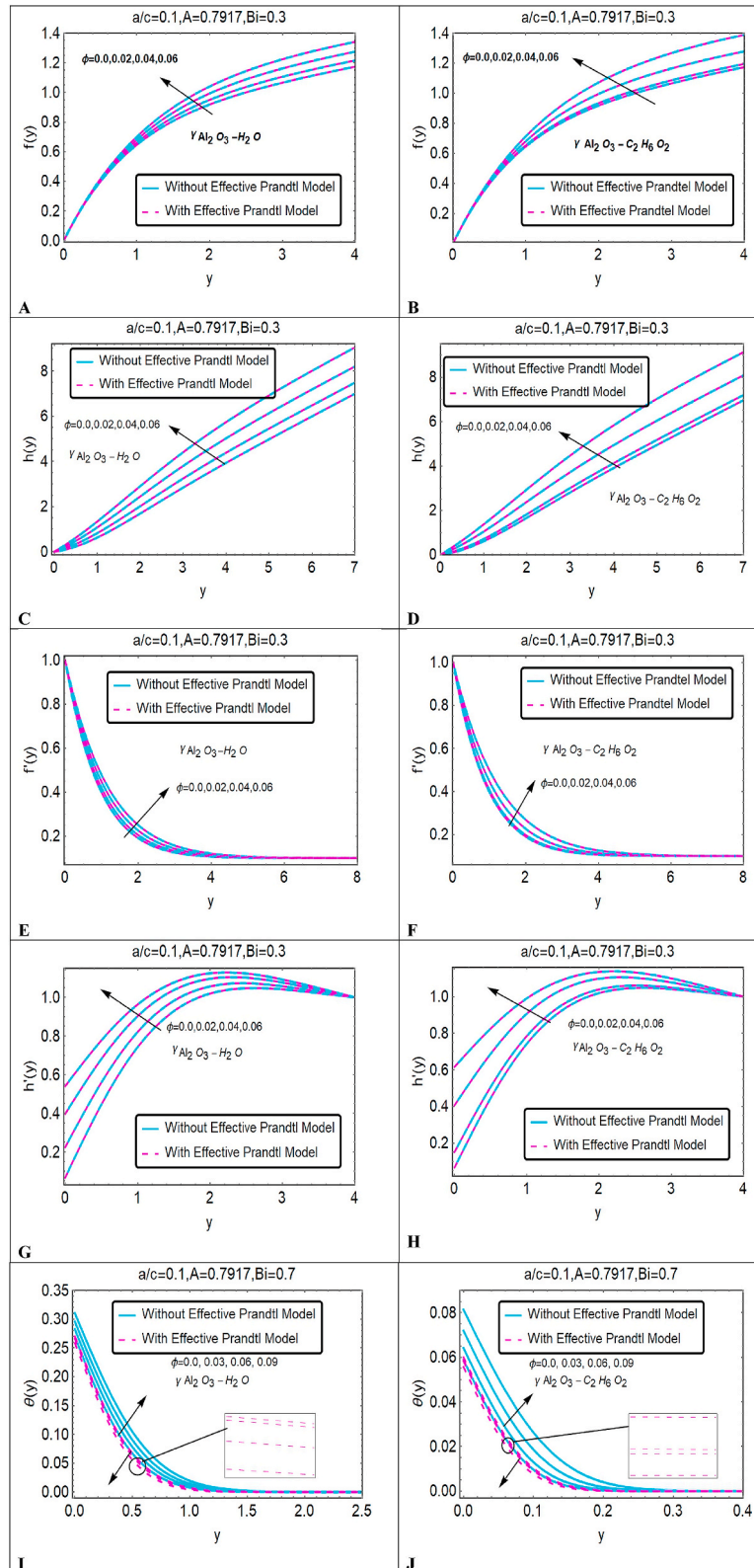


Fig. 3. (A–J): Impact of Nanoparticles Volume fraction  $\phi$  on  $f(y), h(y), f'(y), h'(y)$  and  $\theta(y)$  for  $\gamma Al_2O_3 - H_2O$  and  $\gamma Al_2O_3 - C_2H_6O_2$ .

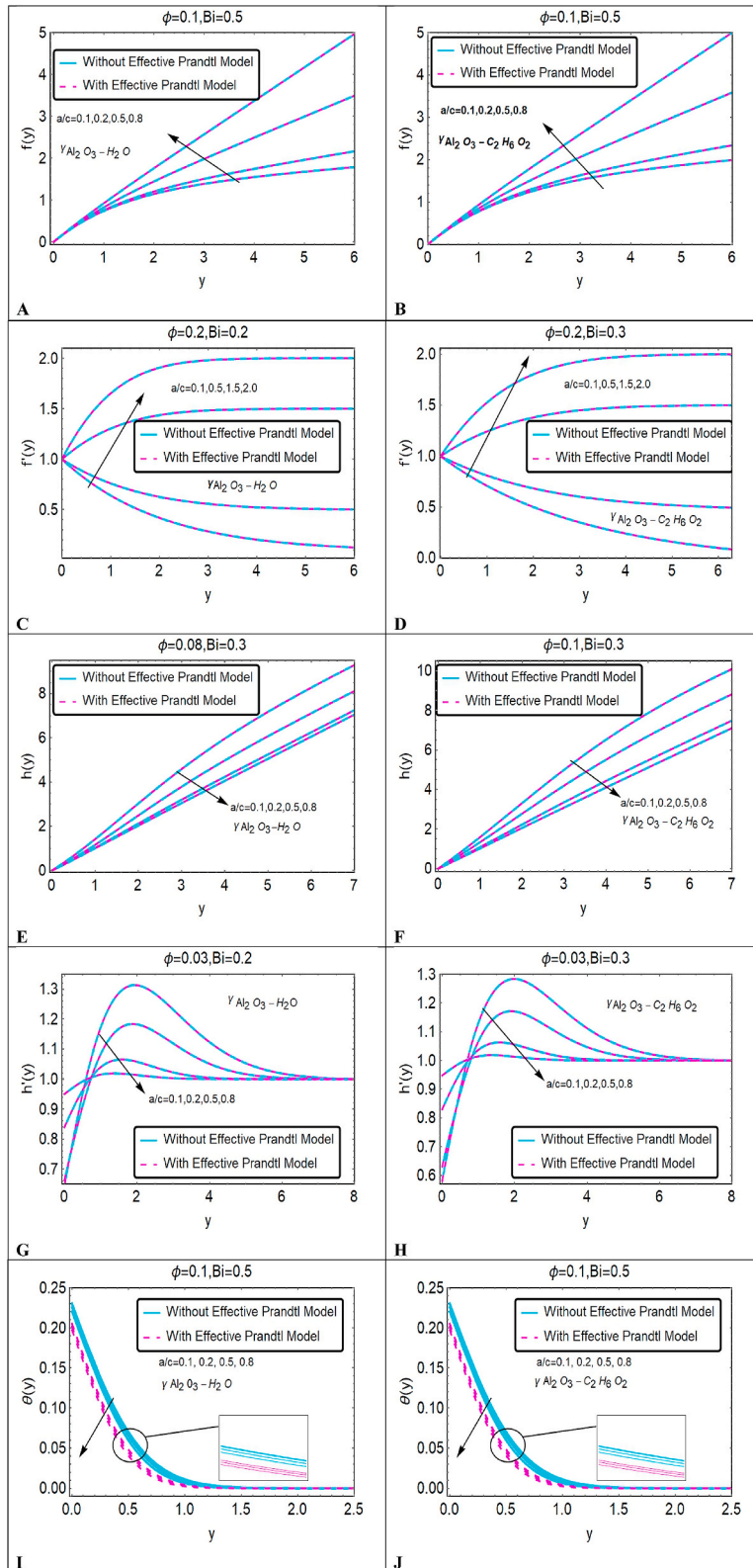


Fig. 4. (A–J): Impact of  $\frac{a}{c}$  on  $f(y), h(y), f'(y), h'(y)$  and  $\theta(y)$  for  $\gamma Al_2O_3 - H_2O$  and  $\gamma Al_2O_3 - C_2H_6O_2$ .

Where  $\gamma$  controls the obliqueness of the flow.

### 3. Mathematical analysis

Intense difficulty arises when attempting to solve a set of nonlinear partial differential equations 20–22 with related boundary conditions (23). To solve these equations, a numerical approach would be preferable. A shooting approach combined with a 4th order Runge Kutta Fehlberg integration structure and boundary conditions (23) makes it feasible to numerically solve the transformed system of equations 20–22. Using the shooting approach, boundary value problems are transformed into a collection of nonlinear 1st order ordinary differential equations (ODEs) with specified initial conditions, which can then be solved numerically. Step size  $\Delta\eta = 0.001$  is employed as a criterion of convergence in order to arrive at a numerical solution with accuracy to the fifth decimal place with a  $\eta_{max} = 20$ .

It is proposed to make the following replacements in the governing ODEs:

$$Y_1 = f, Y_2 = f', Y_3 = f'', Y_4 = h, Y_5 = h', Y_7 = \theta, Y_8 = \theta', \tag{27}$$

using equation (27),

$$Y'_1 = f', Y'_2 = f'', Y'_3 = YY_1 = f''', Y'_4 = h', Y'_5 = YY_5 = h'', Y'_7 = \theta', YY_8 = \theta'', \tag{28}$$

The following is a list of the outcomes that we obtained via the use of equations (27) and (28) (See Ref. [1]).

$$Y'_1 = Y_2, Y'_2 = Y_3, YY_1 = f''', Y'_4 = Y_5, Y'_5 = YY_5 = h'', Y'_7 = Y_8, YY_8 = \theta'', \tag{29}$$

The following are the preliminary conditions for a number of 1st order ordinary differential equations (see Refs. [1,27])

$$YY_1 = -\dot{A} \left[ (1 - \varphi) + \varphi \frac{\rho_s}{\rho_t} \right] (Y_1 Y_3 - Y_2^2) + \left( \frac{a}{c} \right)^2, \tag{30}$$

$$YY_5 = -\dot{A} \left[ (1 - \varphi) + \varphi \frac{\rho_s}{\rho_f} \right] (Y_1 Y_5 - Y_2 Y_4 - A) = 0, \tag{31}$$

$$YY_8 = -\overline{\mathcal{H}}(Y_1 Y_8). \tag{32}$$

$$\left. \begin{aligned} Y_1(0) = 0, Y_2(0) = 1, Y_3(0) = 0, Y_8(0) = -j_2(1 - Y_7(0)), \\ Y_4(0) = j_1, Y_5(0) = 1, Y_9(0) = 0 \end{aligned} \right\} \tag{33}$$

With regard to the provided free stream circumstances, the shooting parameters  $j_1$  and  $j_2$  are first-guess estimates, which are subsequently calculated using Newton-Raphson’s approach for each variable. The numerical solution to the initial value problem that emerges will be accomplished by the use of Runge–Kutta–Fehlberg integration technique implemented in a sophisticated computational software package known as Mathematica [1]. It is one of the sorts that are used in business, and the reason for this is that it recognizes the foremost organization and makes use of the extremely appropriate mathematical approach to deliver proper answers for the system.

### 4. Analysis and discussion of results

The ongoing employment, which is concerned with oblique stagnation point flow, is focused on nanofluids that include ( $H_2O$  and  $C_2H_6O_2$ ) as a base fluid and  $\gamma Al_2O_3 - H_2O$  and  $\gamma Al_2O_3 - C_2H_6O_2$  nanoparticles as nanoparticle transports. The flow has been studied

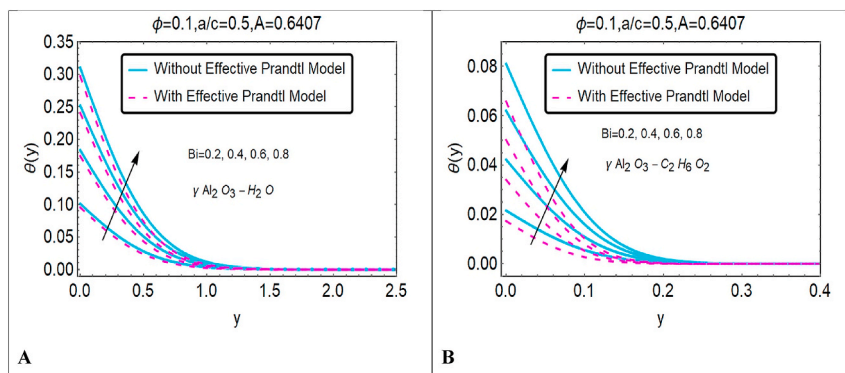


Fig. 5. (A–B): A depiction of the temperature variation  $\theta(y)$  in comparison to  $Bi$  for  $\gamma Al_2O_3 - H_2O$  and  $\gamma Al_2O_3 - C_2H_6O_2$ .

in relation to the Prandtl number. The numerical solution of the linked nonlinear system of ODEs, together with the related starting conditions, is addressed in the preceding section. Graphical representations of how normal courses of flow, temperature, and velocity profiles, streamline patterns, skin friction coefficients, and the local thermal efficiency are affected by different physical factors are shown and evaluated. There are two types of nanofluids studied in detail  $\gamma Al_2O_3 - H_2O$  and  $\gamma Al_2O_3 - C_2H_6O_2$ . Including both situations, graphical representation of flow, velocity, temperature profiles and streamline patterns are analyzed in detail. Consideration is given to a wide range of variables while calculating the flow, velocity, streamline patterns and temperature profiles in both situations, as represented graphically in Figs. 3–7. Skin friction coefficient, Nusselt number and zero wall of stagnation points are shown in Tables 5–8. The boundary layer thickness  $\eta_\infty = 20$  and prior to making comparisons with the previous scenario, the Prandtl number for water was  $Pr = 6.96$ , and for ethylene glycol was  $Pr = 20.4$  is fixed. The control parameters values such as  $0 \leq \phi \leq 0.2$ ,  $0 \leq a/c \leq 2$  and  $0 \leq Bi \leq 1.0$  have been adjusted as shown in the tables and graphs. This research selects control parameter values that were shown to be appropriate within the range of these parameters that had been investigated in earlier studies by Nadeem et al. [21] and Ramzan et al. [8].

4.1. Analysis of results

This section investigates the performance of normal  $f(y)$  and velocity  $f'(y)$ , tangential flow  $h(y)$  and velocity  $h'(y)$ , temperature profile  $\theta(y)$ , and streamline patterns in relation to the effects of different parameters for  $\gamma Al_2O_3 - H_2O$  and  $\gamma Al_2O_3 - C_2H_6O_2$  nanofluid. The several iterations of Fig. 3 (A–H) are shown by their respective values of  $\phi$  on  $\gamma Al_2O_3 - H_2O$  and  $\gamma Al_2O_3 - C_2H_6O_2$  for normal flow  $f(y)$  and velocity  $f'(y)$ , tangential flow  $h(y)$  and velocity  $h'(y)$ , and temperature  $\theta(y)$  profiles. It has been established that the normal  $f(y)$  and tangential flow  $h(y)$  and normal  $f'(y)$  and tangential  $h'(y)$  velocity profiles in Fig. 3 are observed to soar with augmentation in the values of  $\phi$  for the models without and with effective Prandtl numbers. The temperature profiles in Fig. 3(I) and (J) and , on the other hand, exhibit opposite behavior against  $\phi$  for with and without an effective Prandtl number model.

As seen in Fig. 4 (A–J), the stretching ratio  $a/c$  on  $\gamma Al_2O_3 - H_2O$  and  $\gamma Al_2O_3 - C_2H_6O_2$  nanofluids for normal flow  $f(y)$ , and velocity  $f'(y)$ , tangential flow  $h(y)$  and velocity  $h'(y)$ , and temperature  $\theta(y)$  profiles. It is observed that the normal flow  $f(y)$  as well as velocity  $f'(y)$  profiles in Fig. 4(A), (B), Fig. 4(C), and Fig. 4(D) are found to boost up with upsurges of  $a/c$ . By contrast, increasing the values of the stretching ratio parameter  $a/c$  results in a reduction in the tangential profiles  $h(y)$  and  $h'(y)$  seen in Fig. 4(E) and (F), Fig. 4(G) and (H). By increasing the stretching ratio parameter  $a/c$ , the temperature profiles  $\theta(y)$  on  $\gamma Al_2O_3 - H_2O$  and  $\gamma Al_2O_3 - C_2H_6O_2$  nanofluids shown in Fig. 4(I) and (J) and continue to show a downward trend for without and with effective Prandtl number model.

Fig. 5(A) and (B) and show the effect of the Biot number  $Bi$  on the temperature profile  $\theta(y)$  of  $\gamma Al_2O_3 - H_2O$  and  $\gamma Al_2O_3 - C_2H_6O_2$  nanofluids, respectively. Fig. 5 increases with an increase in the Biot number  $Bi$ . In the case of the oblique flows, the streamline patterns  $\gamma Al_2O_3 - H_2O$  and  $\gamma Al_2O_3 - C_2H_6O_2$  nanofluids are demonstrated in Figs. 6 and 7, for diverse values of  $\gamma$ . It has been noticed that the point of stagnation is located to the left of the origin when the value of  $\gamma$  is positive, but when the value of  $\gamma$  is negative, the point of stagnation is located to the right of the origin.

4.2. Discussion of results

To numerically solve the coupled equations (20)–(22) as well as the boundary conditions (23), the RK-IV scheme from the

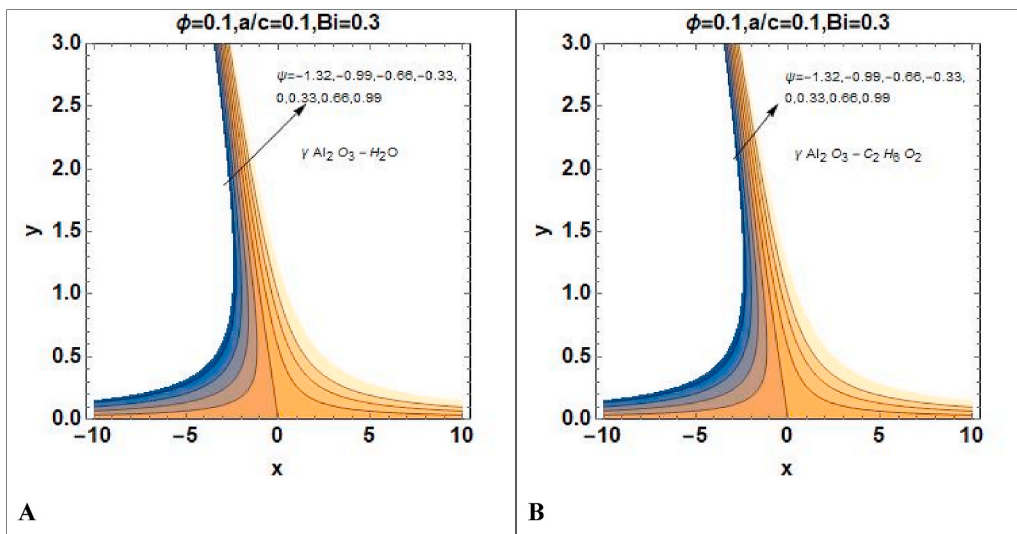


Fig. 6. (A–B): Streamlines patterns when  $\gamma = 2.0$  for  $\gamma Al_2O_3 - H_2O$  and  $\gamma Al_2O_3 - C_2H_6O_2$ .

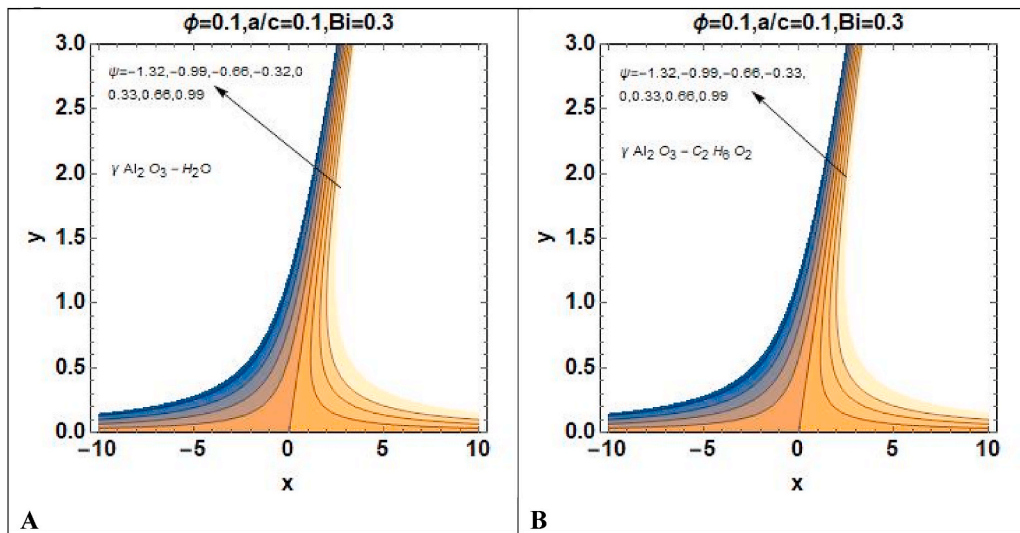


Fig. 7. (A–B): Streamlines patterns when  $\gamma = -2.0$  for  $\gamma Al_2O_3 - H_2O$  and  $\gamma Al_2O_3 - C_2H_6O_2$ .

Table 4

Comparative analysis with previously published material when  $\varphi = 0$ .

	$f''(0)$			$h'(0)$		
$a/c$	Present	Nadeem et al. [27]	Ramzan et al. [8]	Present	Nadeem et al. [27]	Ramzan et al. [8]
0.1	- 0.96935	- 0.96938	- 0.96930	0.26343	0.26341	0.36339
0.2	- 0.918108			0.46876		
0.5	- 0.667264			0.782674		
0.8	- 0.29937	- 0.29938	- 0.29935	0.934767	0.93473	0.93471
1.2	0.337739			1.04919		

Table 5

Local skin friction coefficients calculated numerically for  $\gamma Al_2O_3 - H_2O$  and  $\gamma Al_2O_3 - C_2H_6O_2$ .

$\varphi$	$a/c$	A	Bi	$\gamma Al_2O_3 - H_2O$		$\gamma Al_2O_3 - C_2H_6O_2$	
				$\frac{\mu_{nf} f''(0)}{\mu_f}$	$\frac{\mu_{nf} h'(0)}{\mu_f}$	$\frac{\mu_{nf} f''(0)}{\mu_f}$	$\frac{\mu_{nf} h'(0)}{\mu_f}$
0.01	0.1	0.7917	0.5	1.02482	0.387514	0.995691	0.267512
0.05	-	-	-	1.34382	1.51375	1.63534	1.75204
0.1	-	-	-	1.90084	4.059	2.18717	5.99305
0.2	-	-	-	3.34206	10.6646	4.4193	16.764
0.1	-	-	-	1.90084	4.059000	2.18717	5.99305
-	0.2	0.6407	-	1.79962	3.30037	2.06931	5.03907
-	0.5	0.3286	-	1.30776	2.91505	1.50306	4.21911
-	0.8	0.1145	-	0.586766	2.92846	0.674368	4.06572

Mathematica package is used. In order to validate the reliability of the findings, a comparison was carried out with the data that had been presented in Table 4 earlier. On the other hand, the numerical approach that was established in this article may not be able to provide relevant findings in certain circumstances. For instance, the similarity transformation is used in order to find solutions to the governing equations that are posed in this study. Because of this, it is essential that each of the resultant parameters in this investigation remain unchanged. These parameters include the nanoparticle volume fraction  $\varphi$ , the velocity ratio parameter  $a/c$ , and the Biot number  $Bi$ . It is impossible for the controlling parameter to permit the similarity equation, which leads to the production of findings that cannot be relied upon. Looking at the produced profiles is still another approach one may use in order to evaluate the precision of the numerical technique that was applied in this investigation. In the event that the profiles do not converge asymptotically, this indicates that the boundary condition (23) is not being met. As a consequence, we are forced to come to the realization that the findings were, indeed, not significant.

All the preceding measurements of the parameters that regulate the system for flow  $f(y)$  and  $h(y)$ , velocities  $f'(y)$  and  $h'(y)$ , and temperature  $\theta(y)$  profiles as well as streamline patterns that were reported in Section 4.1 are going to be validated in this section.

The normal flow  $f(y)$ , velocity  $f'(y)$ , and tangential flow  $h(y)$  and velocity  $h'(y)$ , as well as the temperature  $\theta(y)$  profiles in Fig. 3 (A-

**Table 6**  
Local Nusselt numbers calculated numerically for  $\gamma Al_2O_3 - H_2O$  and  $\gamma Al_2O_3 - C_2H_6O_2$ .

$\varphi$	$a/c$	$A$	$Bi$	$\gamma Al_2O_3 - H_2O$		$\gamma Al_2O_3 - C_2H_6O_2$	
				With effective Prandtl No	Without effective Prandtl No	With effective Prandtl No	Without effective Prandtl No
				$-\frac{k_{nf}\theta'(0)}{k_f}$	$-\frac{k_{nf}\theta'(0)}{k_f}$	$-\frac{k_{nf}\theta'(0)}{k_f}$	$-\frac{k_{nf}\theta'(0)}{k_f}$
0.01	0.1	0.7917	0.3	0.26622	0.265742	0.301242	0.301154
0.05	–	–	–	0.297407	0.294834	0.354395	0.353702
0.1	–	–	–	0.343305	0.336103	0.459365	0.456387
0.2	–	–	–	0.457646	0.43341	0.797309	0.782637
0.1	–	0.7917	–	0.343305	0.336103	0.459365	0.456387
–	0.2	0.6407	–	0.343514	0.336380	0.459371	0.456397
–	0.5	0.3286	–	0.344423	0.337565	0.459403	0.456446
–	0.8	0.1145	–	0.345561	0.339011	0.459448	0.456516
–	0.1	0.7917	0.2	0.239586	0.236056	0.285749	0.307551
–	–	–	0.4	0.438142	0.426479	0.524144	0.602087
–	–	–	0.6	0.605377	0.587755	0.728529	0.884589
–	–	–	0.8	0.748161	0.721428	0.908212	1.15601

**Table 7**  
Numerical estimates of  $x_s$  of  $\tau_w$  for varying numbers of  $\varphi$  and  $a/c$ . When  $\gamma = 2$  for  $\gamma Al_2O_3 - H_2O$  and  $\gamma Al_2O_3 - C_2H_6O_2$

$\varphi$	$a/c$	$A$	$Bi$	$\gamma Al_2O_3 - H_2O$	$\gamma Al_2O_3 - C_2H_6O_2$
				$x_s = -\gamma \frac{h'(0)}{f''(0)}$	$x_s = -\gamma \frac{h'(0)}{f''(0)}$
0.01	0.1	0.7917	0.5	0.756258	0.53734
0.05	–	–	–	2.2529	2.56875
0.1	–	–	–	4.27074	5.4802
0.2	–	–	–	6.38205	7.58673
0.1	–	–	–	4.27074	5.4802
–	0.5	0.3286	–	4.45808	5.61404
–	0.8	0.1145	–	9.9817	12.0579

**Table 8**  
Numerical values of  $x_s$  of  $\tau_w$  for distinct estimates of  $\varphi$  and  $a/c$ . When  $\gamma = -2$  for  $\gamma Al_2O_3 - H_2O$  and  $\gamma Al_2O_3 - C_2H_6O_2$ .

$\varphi$	$a/c$	$A$	$Bi$	$\gamma Al_2O_3 - H_2O$	$\gamma Al_2O_3 - C_2H_6O_2$
				$x_s = -\gamma \frac{h'(0)}{f''(0)}$	$x_s = -\gamma \frac{h'(0)}{f''(0)}$
0.01	0.1	0.7917	0.5	-0.756258	-0.53734
0.05	–	–	–	-2.2529	-2.56875
0.1	–	–	–	-4.27074	-5.4802
0.2	–	–	–	-6.38205	-7.58673
0.1	–	–	–	-4.27074	-5.4802
–	0.5	0.3286	–	-4.45808	-5.61404
–	0.8	0.1145	–	-9.9817	-12.0579

H), all increase in magnitude as the volume fraction  $\varphi$  of  $\gamma Al_2O_3 - H_2O$  and  $\gamma Al_2O_3 - C_2H_6O_2$  nanofluid increases. Increasing the volume fraction  $\varphi$  of  $\gamma Al_2O_3 - H_2O$  and  $\gamma Al_2O_3 - C_2H_6O_2$  results in the opposite behavior without and with an effective Prandtl number model. Streamlined patterns also become more pronounced. Similar results were reported by Nadeem et al. [21] for Fig. 3 (A) and 3 (B), and Fig. 3 (E). The increase in quantity results in a drop in the density of the nanofluid that is being considered, which leads to a rise in the flow rate as a direct consequence of the velocity. As a result, the inter-molecular forces that hold the particles of nanofluids together become less strong, and as a direct consequence of this, the flow of the fluid and its velocity quicken. It is obvious that the  $\gamma Al_2O_3 - C_2H_6O_2$  has significantly higher flow and velocity than the  $\gamma Al_2O_3 - H_2O$ . The presence of effective  $Pr$  increases the thickness of the nano momentum boundary layer. Because the expression used for the effective  $Pr$  number model contains density in its denominator, increasing the number of nanoparticles decreases density, which in turn increases the momentum boundary layer thickness.

In order to provide an answer to the second research question, Fig. 3(I) and (J) illustrate the impact that  $\varphi$  has on the temperature profile  $\theta(y)$ . The nanoparticle volume fraction parameter, denoted by the letter "  $\varphi$  " has a significant effect on  $\gamma Al_2O_3 - H_2O$  and  $\gamma Al_2O_3 - C_2H_6O_2$  nanofluid temperature. In the absence of an effective Prandtl number model, increasing the values of the nanoparticle volume fraction parameter  $\varphi$  increases the temperature profile while decreasing the thickness of the nanothermal boundary layer for  $\gamma Al_2O_3 - H_2O$  and  $\gamma Al_2O_3 - C_2H_6O_2$  (Fig. 3(I) and (J)). The equations that are utilized without an effective Prandtl number

are  $\overline{\mathcal{H}} = \frac{Pr_f \left( 1 - \varphi + \varphi \left( \frac{(\mu C_p)_s}{(\mu C_p)_f} \right) \right)}{4.97\varphi^2 + 2.72\varphi + 1}$  and  $\frac{Pr_f \left( 1 - \varphi + \varphi \left( \frac{(\mu C_p)_s}{(\mu C_p)_f} \right) \right)}{28.905\varphi^2 + 2.8273\varphi + 1}$ , correspondingly, for  $\gamma Al_2O_3 - H_2O$  and  $\gamma Al_2O_3 - C_2H_6O_2$  nanofluids. Each of these formulations contains the thermal conductivity component in its denominator. The primary explanation for this phenomenon is that an increase in the value of  $\varphi$  raises the thermal conductivity of the fluid, which in turn causes an increase in temperature for models that do not include an effective Prandtl number. When there is effective  $Pr$  present, the temperature profile decreases as the values of  $\varphi$

increase. The terms  $\overline{\mathcal{H}} = \frac{Pr_f \left( (1-\varphi) + \varphi \frac{\mu_s}{\mu_f} (82.1\varphi^2 + 3.9\varphi + 1) \right)}{123\varphi^2 + 7.3\varphi + 1}$  and  $\overline{\mathcal{H}} = \frac{Pr_f \left( (1-\varphi) + \varphi \frac{\mu_s}{\mu_f} (254.3\varphi^2 - 3\varphi + 1) \right)}{306\varphi^2 - 0.19\varphi + 1}$  for  $\gamma Al_2O_3 - H_2O$  and  $\gamma Al_2O_3 - C_2H_6O_2$  nanofluids are included in the formulas for the effective Prandtl number. These formulations are used to calculate the effective Prandtl number. These phrases, as one can see, include the ratio of the viscosity of the substance. Because high values of  $\varphi$  reduce the viscosity of nanofluids, which in turn results in an increase in the thickness of the nanothermal boundary layer for models that use an effective Prandtl number, the physical explanation for this phenomenon is as follows: When looking at these figures, one can see that the nanothermal boundary layer thickness of  $\gamma Al_2O_3 - H_2O$  and  $\gamma Al_2O_3 - C_2H_6O_2$  decreases when effective  $Pr$  is not present, whereas the nanothermal boundary layer thickness of  $\gamma Al_2O_3 - H_2O$  and  $\gamma Al_2O_3 - C_2H_6O_2$  increases when effective  $Pr$  is present. Because an equation using an efficient Prandtl number model requires consideration of both the density of the surface and the density of the fluid, the densities of the thermal boundary layer are directly related to one another in an inverse fashion. Therefore, a lower thermal boundary layer results from an increase in density. Expressions that do not use the effective Prandtl number involve thermal conductivity; hence, when the values of  $\varphi$  grow, thermal conductivity also increases, which results in a drop in the thermal boundary layer. Fig. 3(I) and (J) and clearly show that when gamma alumina is combined with water, the temperature rises, whereas when gamma alumina is combined with ethylene glycol, the temperature falls. The reason for this conclusion is because  $H_2O$  has a lower Prandtl number ( $Pr$ ) than  $C_2H_6O_2$ , and consequently, the thermal diffusivity of  $H_2O$  is significantly superior to that of  $C_2H_6O_2$ . In this instance of  $\gamma Al_2O_3 - C_2H_6O_2$ , the model without an effective Prandtl number has a better temperature profile. Nanofluids based on  $C_2H_6O_2$  might also be employed for cooling applications which is another use for them.

The free stream velocity is used to determine the stretching ratio parameter, which is defined as the stretching velocity divided by the free stream velocity. As a result, for a constant value of  $a/c$  related to the stretching of the employed surfaces, the increase in a proportion to  $c$  implies an increase in straining movements near the stagnation region, which may increase the external stream's acceleration. This is the primary reason for the increase in normal flow and velocity shown in Fig. 4 (A-D). On other hand, the tangential profile shown in Fig. 4 (E-H) displays the opposite tendency. This is due to the fact that it is parallel to the  $x-$  axis, and the amount of stretching that occurs parallel to the  $x-$  axis is  $c$ . This value is included in the denominator of the stretching ratio parameter. The tangential velocity decreases when the value of the stretching parameter is increased. When the stretching ratio parameter  $a/c$  in Fig. 4 (I-J) is increased, the further temperature profile decreases in the same way for both models (with and without effective  $Pr$ ). In both the  $\gamma Al_2O_3 - H_2O$  and  $\gamma Al_2O_3 - C_2H_6O_2$  nanofluid situations, comparative research shows that the presence of an effective number model has a smaller impact than the absence of such a model. The reason for this is due to the fact that the mathematical equation for the effective  $Pr$  number model involves the viscosity of nanoparticles, which enhances the nanothermal boundary layer and decreases temperature distribution. The temperature profile of the nanofluid containing  $\gamma Al_2O_3$  and  $H_2O$  displays a more significant trend toward a decreasing temperature. Because the nanofluid  $\gamma Al_2O_3 - H_2O$  has a temperature profile that is much lower than that of other fluids, it will not be suitable for use in solar thermal systems of the future. Furthermore  $\gamma Al_2O_3 - C_2H_6O_2$  offer higher normal flow and velocity profiles than  $\gamma Al_2O_3 - H_2O$ . Similar results can be seen by Ramzan et al. [8] for Fig. 4(I) and (J) and . In Fig. 4 (A-H), the incorporation of effective  $Pr$  results in an increase in the nanomomentum boundary layer thickness of both the  $\gamma Al_2O_3 - H_2O$  and  $\gamma Al_2O_3 - C_2H_6O_2$  nanofluids. In Fig. 4 (I) and 4 (J), an increase in the effective Prandtl number also results in a thicker nano thermal boundary layer.

Fig. 5(A) and (B) and show variations in the temperature distribution  $\theta(y)$  profiles of  $\gamma Al_2O_3 - H_2O$  and  $\gamma Al_2O_3 - C_2H_6O_2$  with various Biot numbers  $Bi$  approaching the convective surface. The biot numbers have a mathematical definition, and a rise in their values indicates an increase in the convective heat transfer coefficient. This, in turn, makes it possible for an increased amount of heat to be transferred from the surface. Using the Biot number, one may determine the surface's conduction resistance ratio based on its convection resistance. As shown in Fig. 5(A) and (B) and , increasing the Biot number correlates with improved convective heating, which effectively raises the fluid temperature in the resolution. As the importance increases, there is an increase in the peak height of the temperature distribution profile; hence, an increasing Biot number designates a superior internal thermal resistance of the surface as opposed to the boundary layer thermal resistance. Without an effective Prandtl number model, the temperature profile in Fig. 5(A) and (B) and is higher. Because an effective  $Pr$  model contains an expression in which the thermal conductivity of nanofluid is present. The temperature profile of  $\gamma Al_2O_3 - H_2O$  is significantly greater than that of  $\gamma Al_2O_3 - C_2H_6O_2$ . Ethylene glycol has a poorer heat conductivity than water, which accounts for this. The thickness of the nanothermal boundary layer gets thicker when an effective  $Pr$  number model is used. This is true for both  $\gamma Al_2O_3 - H_2O$  and  $\gamma Al_2O_3 - C_2H_6O_2$  nanofluids.

Figs. 6 and 7 show the behavior of streamline patterns for  $\gamma Al_2O_3 - H_2O$  nanofluid and  $\gamma Al_2O_3 - C_2H_6O_2$  nanofluid, respectively. In these figures, we have explored two distinct examples of the shear stream parameter ( $\gamma = -2.0, \gamma = 2.0$ ) in regard to the pre-determined values of  $\varphi = 0.1, a/c = 0.1$  and  $Bi = 0.5$  on  $\gamma Al_2O_3 - H_2O$  and  $\gamma Al_2O_3 - C_2H_6O_2$  nanofluid, correspondingly. It can be seen very clearly in Fig. 6(A) and (B), which show two plots of streamlines, that in the case when the shear stream parameter  $\gamma$  has a positive value, it is possible to produce an oblique configuration of streamlines for gamma alumina-water and gamma alumina-ethylene glycol, and the distributing streamline strikes the outward at the left side of the origin. These results can be found in both of these figures. Because of this, we were able to deduce that the stagnation point occurs at  $x < 0$  for shear stream parameters with positive values, which means that  $\gamma > 0$ . Furthermore, when  $\gamma = -2.0$ , the streamlines shape becomes crooked once more

additionally, the stream that is separating hits the surface from the positive side, which is where it originated. This can be seen in the final two plots of the streamlines in Fig. 7 (A) and 7 (B), respectively. Because of this, we were able to deduce that when the shear stream parameter  $\gamma$  has negative values, i.e.,  $\gamma < 0$ , the stagnation point occurs where  $x > 0$ . According to these findings, the obliquity of flow grows farther and farther when the values of alpha are increased in both positive and negative directions.

#### 4.3. Table discussion

Also, in some cases, a comparison is made between the results that are currently being calculated and the literature that is already available. This is done to make sure that the results that are currently being calculated are accurate compared to the data that has already been published. This assessment is done in order to ensure that the existing determined findings are valid. In order to determine whether or not the mathematical model that has been provided is accurate, Table 4 has been constructed and compared in conjunction with the work of Nadeem et al. [27] and Ramzan et al. [8] over a broad range of possible values of  $a/c$  in the limiting scenario. Nadeem et al. [27] used built in function in MAPLE whereas Ramzan et al. [8] used bvp4c in MATLAB while in present research we used RK-IV with shooting techniques in MATHEMATICA. There has been a very strong relationship discovered between the values.

The development of tables [5,6] was necessitated by the need to handle physical aspects that were significant, such as  $\tau_w$  aspects as well as  $q_w$  at the convective stretching surface, regardless of whether a Prandtl number was efficient or not. It is evident from these data that the normal  $\frac{\mu_{nf} f''(0)}{\mu_f}$  and tangential  $\frac{\mu_{nf} h'(0)}{\mu_f}$  skin friction and local heat transfer ( $q_w$ ) aspects grow with increasing volume fraction in both  $\gamma Al_2O_3 - H_2O$  and  $\gamma Al_2O_3 - C_2H_6O_2$  nanofluids studied. Tables 5 and 6 show, respectively, how the nanoparticle volume fraction  $\varphi$  toward the convective surface influences normal and tangential skin friction as well as the local Nusselt number. It has been shown that there is a correlation between an intensification in the amount of  $\varphi$  and a rise in the significance of both the local heat transfer rate  $q_w$  and the shear stress. The collisions that take place between nanoparticles and the fragments that make up the support fluid cause the fluid's velocity to rise when it contains nanoparticles. This increase in fluid velocity is affected by the occurrence of nanoparticles in the base fluid. Nanoparticles are responsible for triggering this event when they are present. As a consequence of this, the height of the momentum boundary layer will become thinner, which eventually lead to an increase in the amount of normal and tangential skin friction and heat transfer at the surface. In Table 5, one can see that with increasing values of  $\varphi$ , gamma alumina ethylene glycol has a greater normal and tangential skin friction component than gamma alumina water, regardless of the effective Prandtl number. Table 6 reveal that with increasing values of  $\varphi$ ,  $\gamma Al_2O_3 - H_2O$  nanofluid shows better heat transfer than  $\gamma Al_2O_3 - C_2H_6O_2$  nanofluid for with effective Prandtl number model. Reason behind this is that  $H_2O$  has higher thermal conductivity than  $C_2H_6O_2$ . Also note that with effective Prandtl number model has higher heat transfer rate than without effective Prandtl number model for  $\gamma Al_2O_3 - H_2O$  nanofluid and  $\gamma Al_2O_3 - C_2H_6O_2$  for some values of  $\varphi$ . The viscosity of nanoparticles is included in the mathematical formula that is utilized for the effective  $Pr$  model, as is clear to everyone who looks at it. Because an equation using an efficient Prandtl number model requires consideration of both the density of the surface and the density of the fluid, The densities of the thermal boundary layer are directly related to one another in an inverse fashion. Therefore, a thinner thermal boundary layer results from an increase in density, which in turn leads to an increase in the rate of heat transmission. Increasing the stretching ratio has also been reported to decrease skin friction in both the normal and tangential directions. Nanofluids made of both  $\gamma Al_2O_3 - H_2O$  and  $\gamma Al_2O_3 - C_2H_6O_2$  display the same properties. The magnitude of skin friction in both normal and tangential directions shows that  $\gamma Al_2O_3 - C_2H_6O_2$  has good impact than  $\gamma Al_2O_3 - H_2O$  nanofluid. For both  $\gamma Al_2O_3 - H_2O$  and  $\gamma Al_2O_3 - C_2H_6O_2$  nanofluids local heat flux is shown in Table 6. Both types of nanofluids experience an upsurge in volume friction-induced heat flux at the stretched convective surface whether they have an effective Prandtl number or not. The magnitudes of local heat transfer rate in Table 6 show that without an effective Prandtl number, there is less impact than with an effective Prandtl number for  $\gamma Al_2O_3 - H_2O$  and  $\gamma Al_2O_3 - C_2H_6O_2$  nanofluid. The energy equation for the effective Prandtl number model contains an expression in which nanofluid viscosity is included. The increase in stretching quantity results in a drop in the density of the nanofluid that is being considered, which leads to a rise in the heat transfer rate. As a result, the inter-molecular forces that hold the particles of nanofluids together become less strong, and as a direct consequence of this, the rate of heat transfer quickens.

Table 6 depicts the variations in heat transfer rate caused by the value of the Biot number  $Bi$  for the convectively heated stretched surface on  $\gamma Al_2O_3 - H_2O$  and  $\gamma Al_2O_3 - C_2H_6O_2$  nanofluid with and without an effective Prandtl number model. These variations take place in both cases where the effective Prandtl number model was used. This table demonstrates that there is an overall upward tendency in the rate of heat transfer of the systems, which correlates with the rise in the values of  $Bi$ . This trend is shown by the fact that there is a rising trend in the table. This trend toward higher  $Bi$  values fit with the trend toward a higher heat transfer rate. The Biot number is a symbol for expressing the relationship between the internal resistance to conduction inside a stretched surface and the external resistance to convection on that surface. As can be seen in Table 6, it has been shown that a boost in the Biot number, which would be connected to an efficient process of convective heating, is able to efficiently bring down the temperature of the fluid in the solutions. This may be shown to be the case by noting that the Biot number rises in response to increases in the effectiveness of convective heating. It was decided to make this observation. On the other hand, having a large Biot number doesn't always necessarily indicate that there will be a rise in the internal temperature of the stretched surface in comparison to that of its boundary layer. This is the case because when the value of  $Bi$  grows, it causes a surge in the temperature field profile, it demonstrates that the inner thermal efficiency of the material is lower than if the conditions were different. On the other hand, it is essential to keep in mind that there is a one-to-one correspondence between the Biot number and the efficiency of heat transmission, that is denoted by  $h_f$ , and that as a consequence of this, it has an opposing connection with the thermal efficiency of the subject material that is the focus of the discussion

that is now taking place. This is something that needs to be kept in mind at all times. As a consequence of this, the thermal performance lowers as the Biot number grows, which ultimately results in a high temperature distribution as well as a high heat transfer rate at the surface that has been stretched. According to the information shown in Table 6, the magnitude of the heat transfer rate is greater when an effective Prandtl number model is used as opposed to when an effective Prandtl number model is not used for the values of  $Bi$ . The results of this investigation demonstrate that both with and without a useful Prandtl number, gamma alumina ethylene glycol nanofluids are more promising for quick heat transfer from the stretched convective surface than the gamma alumina water.

Using  $Bi = 0.5$  with certain estimates of  $\varphi$  and  $q_c$ , the standards of the wall's zero-skin-friction or shear stress point of stagnation  $x_s$  are shown in Tables 7,8. With and without an effective Prandtl number of  $\gamma Al_2O_3 - H_2O$  and  $\gamma Al_2O_3 - C_2H_6O_2$ , determines the obliqueness of the flow. Certain quantities of  $\varphi$  and  $q_c$  are correlated with better values of  $\gamma$ , while point  $x_s$  is associated with positive values for both types of nanofluids. On the other hand,  $\gamma Al_2O_3 - H_2O$  and  $\gamma Al_2O_3 - C_2H_6O_2$  behave differently when  $\gamma$  is negative. Obliqueness and straining motion are in harmony, resulting in this effect. However, the values of  $\tau_w$ ,  $q_w$  and zero wall shear stress on point  $x_s$  cannot be compared by Nadeem et al. [27] and Ramzan et al. [8] as the present model consider stimulus of effective Prandtl number model for both fluids. For the future reference, the values of  $\tau_w$ ,  $q_w$  and zero wall skin friction on  $x_s$  the current model is presented in its entirety in Tables 5–8.

## 5. Conclusions

This research has addressed the two-dimensional oblique stagnation point flow of  $\gamma Al_2O_3 - H_2O$  and  $\gamma Al_2O_3 - C_2H_6O_2$  across stretched convective surface for with and without an efficient Prandtl number. Using  $H_2O$  and  $C_2H_6O_2$  as base fluids, we can estimate the normal and tangential skin friction, as well as the local heat flux and vicinity of the zero-skin friction point  $x_s$ , among other things. The following are the most significant findings of this research:

- There is a significant role for the Prandtl number in determining the thermal and momentum stretching layer surfaces.
- The increase in thickness of the nano-momentum boundary layer that results from taking effective  $Pr$  into account.
- In nanofluids made of  $\gamma Al_2O_3 - H_2O$  and  $\gamma Al_2O_3 - C_2H_6O_2$  and ethylene, the thickness of the nanothermal boundary layer grows when effective  $Pr$  is present.
- In the absence of an effective  $Pr$ , the nanothermal boundary layer thickness of  $\gamma Al_2O_3 - H_2O$ , as well as  $\gamma Al_2O_3 - C_2H_6O_2$ , drops.
- For  $\gamma Al_2O_3 - H_2O$  and  $\gamma Al_2O_3 - C_2H_6O_2$ , the magnitude of the skin friction coefficient and the lowered Nusselt number rise in the presence of effective  $Pr$ , leading to rising values of  $\varphi$ . This holds true for both systems. Gamma alumina-water is less resistant to typical skin friction ( $\tau_w$ ) and has a lower heat transfer rate ( $q_w$ ) than gamma alumina ethylene glycol.
- In the presence of an effective  $Pr$  number model, the magnitude of skin friction and the lowered Nusselt number decrease with the stretching ratio parameter for  $\gamma Al_2O_3 - H_2O$  and  $\gamma Al_2O_3 - C_2H_6O_2$  nanofluids. This is the case regardless of which nanofluid is being studied.
- The effective  $Pr$  number model may be used to manage the nanomomentum boundary layer as well as the nanothermal boundary layer.
- The streamlining is more complete, symmetrical, and straightforward in both instances.
- The flow separation dislocation perpetual for both  $\gamma Al_2O_3 - H_2O$  and  $\gamma Al_2O_3 - C_2H_6O_2$  nanofluids exhibited increasing behavioral patterns with volume friction and decreasing stretching ratio. Displacement constants are greater in the case when the solution is composed of gamma-alumina ethylene glycol rather than water.
- For a normal velocity profile, the velocity ratio parameter  $a/c$  has risen, whereas for tangential and temperature profiles, it has reduced.
- In both  $\gamma Al_2O_3 - H_2O$  and  $\gamma Al_2O_3 - C_2H_6O_2$ , the temperature profiles rise when an effective Prandtl number is present for stretching ratio parameter.
- Temperature profile increases for increasing values of biot number for  $\gamma Al_2O_3 - H_2O$  and  $\gamma Al_2O_3 - C_2H_6O_2$  nanofluid for both with and without effective  $Pr$  model.
- $\gamma Al_2O_3 - C_2H_6O_2$  depicted higher  $\tau_w$  and  $q_w$  than  $\gamma Al_2O_3 - H_2O$ .
- Further research has shown that the stretching ratio parameter has an influence on the direction of the point  $x_s$  of zero skin friction (shear stress on the wall). In addition, there are no published analytical or empirical data for evaluation currently.

## 6. Research contribution and future suggestion

The current mathematical modelling may be applicable to the production of materials in industry segments such as thermoplastic layers, crystal production, particles passing between nutrient spools, magnesium pultrusion, air circulation in metallic baths, air circulation on a large metal plate, and many other processes that benefit many different areas of society. In addition, these models may be of use in a great number of other areas that are important to people's everyday lives.

### Future suggestions

- The investigator is free to apply the slip conditions to the same model.

- The present research might be expanded such that it considers the commercial applications of other species' diffusive liquids and nanofluids.
- In the future, the work that is being done now may be expanded to include the unstable scenario.

#### Author contribution statement

Zafar Mahmood, Umar Khan: conceived and designed the experiments; contributed materials and analysis tools.

Sayed M. Eldin: Performed the experiments, wrote the paper.

Amal F. Soliman: Performed the experiments.

Taghreed A. Assiri: analyzed and interpreted the data.

S. R. Mahmoud: analyzed and interpreted the data, wrote the paper.

#### Funding statement

This research did not receive any specific grant from funding agencies in the public, commercial, or not-for-profit sectors.

#### Data availability statement

Data will be made available on request.

#### Declaration of interest's statement

The authors declare no conflict of interest.

#### Acknowledgments

We would like to thank the reviewers for their thoughtful comments and efforts towards improving our paper.

#### References

- [1] Z. Mahmood, N.A. Ahammad, S.E. Alhazmi, U. Khan, M.Z. Bani-Fwaz, Ternary hybrid nanofluid near a stretching/shrinking sheet with heat generation/absorption and velocity slip on unsteady stagnation point flow, *Int. J. Mod. Phys. B* (2022), 2250209.
- [2] B.C. Sakiadis, Boundary-layer behaviour on continuous solid surface: I Boundary-layer equations for two-dimensional and axisymmetric flow, *J. Am. Inst. Chem. Eng.* 7 (1961) 26–28.
- [3] N.H. Sweilam, T.A. Assiri, M.M. Abou Hasan, Numerical solutions of nonlinear fractional Schrödinger equations using nonstandard discretizations, *Numer. Methods Part. Differ. Equ.* 33 (5) (2017) 1399–1419.
- [4] B. Alqahtani, Z. Mahmood, M.A. Alyami, A.M. Alotaibi, U. Khan, A.M. Galal, Heat and mass transfer analysis of MHD stagnation point flow of carbon nanotubes with convective stretching disk and viscous dissipation, *Adv. Mech. Eng.* 14 (10) (2022), 16878132221128390.
- [5] Z. Mahmood, S.E. Alhazmi, U. Khan, M.Z. Bani-Fwaz, A.M. Galal, Unsteady MHD stagnation point flow of ternary hybrid nanofluid over a spinning sphere with Joule heating, *Int. J. Mod. Phys. B* (2022), 2250230.
- [6] Z. Mahmood, Z. Iqbal, M.A. Alyami, B. Alqahtani, M.F. Yassen, U. Khan, Influence of suction and heat source on MHD stagnation point flow of ternary hybrid nanofluid over convectively heated stretching/shrinking cylinder, *Adv. Mech. Eng.* 14 (9) (2022), 16878132221126278.
- [7] N. Sandeep, M. Girinath Reddy, P.A. Dinesh, Effect of temperature-dependent viscosity on hydromagnetic unalined flow, *Proc. Inst. Mech. Eng. Part E J. Process Mech. Eng.* (2022), 09544089221087811.
- [8] M. Ramzan, N. Shahmir, H. Alotaibi, H.A.S. Ghazwani, T. Muhammad, Thermal performance comparative analysis of nanofluid flows at an oblique stagnation point considering Xue model: a solar application, *J. Comput. Des. Eng.* 9 (1) (2022) 201–215.
- [9] J.T. Stuart, The viscous flow near a stagnation point when the external flow has uniform vorticity, *J. Aero. Sci.* 26 (2) (1959) 124–125.
- [10] K. Tamada, Two-dimensional stagnation-point flow impinging obliquely on a plane wall, *J. Phys. Soc. Japan* 46 (1) (1979) 310–311.
- [11] J.M. Dorrepaal, An exact solution of the Navier-Stokes equation which describes non-orthogonal stagnation-point flow in two dimensions, *J. Fluid Mech.* 163 (1986) 141–147.
- [12] M. Reza, A.S. Gupta, Steady two-dimensional oblique stagnation-point flow towards a stretching surface, *Fluid Dynam. Res.* 37 (5) (2005) 334.
- [13] C. Tc, Stagnation-point flow towards a stretching plate, *J. Phys. Soc. Japan* 63 (6) (1994) 2443–2444.
- [14] Y.Y. Lok, N. Amin, I. Pop, Non-orthogonal stagnation point flow towards a stretching sheet, *Int. J. Non Lin. Mech.* 41 (4) (2006) 622–627.
- [15] M. Reza, A.S. Gupta, Some aspects of non-orthogonal stagnation-point flow towards a stretching surface, *Static Dyn. Charact. High-Speed Silicon Carbide Power Transistors 2* (2010) 705–709.
- [16] P.G. Drazin, N. Riley, *The Navier-Stokes Equations: a Classification of Flows and Exact Solutions*, 334, Cambridge University Press, 2006.
- [17] R.M. Tooke, M.G. Blyth, A note on oblique stagnation-point flow, *Phys. Fluids* 20 (3) (2008), 33101.
- [18] P.D. Weidman, V. Putkaradze, Axisymmetric stagnation flow obliquely impinging on a circular cylinder, *Eur. J. Mech. B Fluid* 22 (2) (Mar. 2003) 123–131, [https://doi.org/10.1016/S0997-7546\(03\)00019-0](https://doi.org/10.1016/S0997-7546(03)00019-0).
- [19] P.D. Weidman, V. Putkaradze, Erratum to 'Axisymmetric stagnation flow obliquely impinging on a circular cylinder' [*Eur. J. Mech. B/Fluids* 22 (2)(2003) 123–131], *Eur. J. Mech. Fluids* 6 (24) (2005) 788–790.
- [20] E. Erfani, M.M. Rashidi, A.B. Parsa, The modified differential transform method for solving off-centered stagnation flow toward a rotating disc, *Int. J. Comput. Methods* 7 (4) (2010) 655–670.
- [21] I. Husain, F. Labropulu, I. Pop, Two-dimensional oblique stagnation-point flow towards a stretching surface in a viscoelastic fluid, *Open Phys.* 9 (1) (2011) 176–182.
- [22] T.R. Mahapatra, S.K. Nandy, A.S. Gupta, Oblique stagnation-point flow and heat transfer towards a shrinking sheet with thermal radiation, *Meccanica* 47 (6) (2012) 1325–1335, Aug, <https://doi.org/10.1007/S11012-011-9516-Z>.
- [23] Y.Y. Lok, I. Pop, D.B. Ingham, Oblique stagnation slip flow of a micropolar fluid, *Meccanica* 45 (2) (2010) 187–198.
- [24] A. Ghaffari, T. Javed, F. Labropulu, Oblique stagnation point flow of a non-Newtonian nanofluid over stretching surface with radiation: a numerical study, *Therm. Sci.* 21 (5) (2017) 2139–2153.

- [25] T. Javed, A. Ghaffari, H. Ahmad, Numerical study of unsteady MHD oblique stagnation point flow with heat transfer over an oscillating flat plate, *Can. J. Phys.* 93 (10) (2015) 1138–1143.
- [26] A. Ahmed, M. Khan, J. Ahmed, A. Hafeez, Z. Iqbal, Unsteady stagnation point flow of Maxwell nanofluid over stretching disk with joule heating, *Arabian J. Sci. Eng.* 45 (7) (2020).
- [27] S. Nadeem, R. Mehmood, N.S. Akbar, Oblique stagnation point flow of carbon nano tube based fluid over a convective surface, *J. Comput. Theor. Nanosci.* 12 (4) (2015) 605–612.
- [28] A. Ghaffari, T. Javed, I. Mustafa, Non-linear radiation influence on oblique stagnation point flow of Maxwell fluid, *Rev. Mex. física* 64 (4) (2018) 420–428.
- [29] P.K. Mandal, G.S. Seth, S. Sarkar, A. Chamkha, A numerical simulation of mixed convective and arbitrarily oblique radiative stagnation point slip flow of a CNT-water MHD nanofluid, *J. Therm. Anal. Calorim.* 143 (3) (2021) 1901–1916.
- [30] K. Anantha Kumar, A.C. Venkata Ramudu, V. Sugunamma, N. Sandeep, Effect of non-linear thermal radiation on MHD Casson fluid flow past a stretching surface with chemical reaction, *Int. J. Ambient Energy* (2022) 1–8.
- [31] N. Sandeep, C. Sulochana, G.P. Ashwinkumar, Understanding the dynamics of chemically reactive Casson liquid flow above a convectively heated curved expanse, *Proc. Inst. Mech. Eng. Part C J. Mech. Eng. Sci.* 236 (24) (2022) 11420–11430.
- [32] N. Rathore, Darcy–Forchheimer and Ohmic heating effects on GO-TiO<sub>2</sub> suspended cross nanofluid flow through stenosis artery, *Proc. Inst. Mech. Eng. Part C J. Mech. Eng. Sci.* (2022), 09544062221105166.
- [33] A. Moghadassi, S. Masoud Hosseini, D. Henneke, A. Elkamel, A model of nanofluids effective thermal conductivity based on dimensionless groups, *J. Therm. Anal. Calorim.* 96 (1) (2009) 81–84.
- [34] S. Choi, J. Eastman, *Enhancing Thermal Conductivity of Fluids with Nanoparticles*, 1995.
- [35] N. Rathore, A modified thermal flux model to examine the enhanced heat transmission in hybrid blood flow through artery: a comparison between Maxwell and Oldroyd-B models, *Proc. Inst. Mech. Eng. Part E J. Process Mech. Eng.* (2022), 09544089221128367.
- [36] H. Xu, S.I.U. Khan, U. Ghani, W. Bu, A. Zeb, The influence of effective Prandtl number model on the micropolar squeezing flow of nanofluids between parallel disks, *Processes* 10 (6) (2022) 1126.
- [37] D.S. Maciver, H.H. Tobin, R.T. Barth, Catalytic aluminas I. Surface chemistry of eta and gamma alumina, *J. Catal.* 2 (6) (1963) 485–497.
- [38] T. Maré, O. Sow, S. Halefadi, S. Lebourlout, C.T. Nguyen, Experimental study of the freezing point of  $\gamma$ -Al<sub>2</sub>O<sub>3</sub>/water nanofluid, *Adv. Mech. Eng.* 4 (2012), 162961.
- [39] N.V. Ganesh, A.K.A. Hakeem, B. Ganga, A comparative theoretical study on Al<sub>2</sub>O<sub>3</sub> and  $\gamma$ -Al<sub>2</sub>O<sub>3</sub> nanoparticles with different base fluids over a stretching sheet, *Adv. Powder Technol.* 27 (2) (2016) 436–441.
- [40] M.M. Rashidi, N.V. Ganesh, A.K.A. Hakeem, B. Ganga, G. Lorenzini, Influences of an effective Prandtl number model on nano boundary layer flow of  $\gamma$  Al<sub>2</sub>O<sub>3</sub>-H<sub>2</sub>O and  $\gamma$  Al<sub>2</sub>O<sub>3</sub>-C<sub>2</sub>H<sub>6</sub>O<sub>2</sub> over a vertical stretching sheet, *Int. J. Heat Mass Tran.* 98 (2016) 616–623.